Cage Doubling: Solvent-Mediated Re-equilibration of a [3+6] Prismatic Organic Cage to a Large [6+12] Truncated Tetrahedron

Chloe Stackhouse, Valentina Santolini, Rebecca Greenaway, Marc A. Little, Michael E. Briggs, Kim E. Jelfs, and Andrew I. Cooper

Cryst. Growth Des., **Just Accepted Manuscript** • DOI: 10.1021/acs.cgd.7b01422 • Publication Date (Web): 06 Apr 2018

Cage Doubling: Solvent-Mediated Re-equilibration of a [3+6] Prismatic Organic Cage to a Large [6+12] Truncated Tetrahedron

Chloe J. Stackhouse[†], *Valentina Santolini*[‡], *Rebecca L. Greenaway*[†], *Marc A. Little*[†], *Michael E. Briggs*[†], *Kim E. Jelfs*[‡*] *and Andrew I. Cooper*[†*]

[†] University of Liverpool, Department of Chemistry and Materials Innovation Factory, Crown Street, Liverpool, L69 7ZD, Merseyside, England, UK

[‡] Imperial College London, Department of Chemistry, London, SW7 2AZ, England, UK

KEYWORDS: Organic cages, crystal engineering, single crystal, imine cage

ABSTRACT: We show that a [3+6] trigonal prismatic imine cage can re-arrange stoichiometrically and structurally to form a [6+12] cage with a truncated tetrahedral shape with double the mass of the smaller cage. Molecular simulations rationalize why this rearrangement was only observed for the prismatic [3+6] cage **TCC1** but not for the analogous [3+6] cages, **TCC2** and **TCC3**. Solvent was found to be a dominant factor in driving this rearrangement.

INTRODUCTION

Porous organic cages (POCs) are discrete, shape-persistent molecules that possess an intrinsic void, which is accessible via windows in the cage.[1] In contrast to extended, bonded framework materials, such as metal–organic frameworks (MOFs)[2] and covalent organic frameworks (COFs)[3], POCs are often soluble in common organic solvents, opening up a number of processing options and applications.[4,5,6] The cage packing in the solid state has a profound effect on their properties and this can be controlled by the size and shape of the cage, the functionality present on the outer molecular surface, and the conditions under which the cage is isolated from solvent.[7,8] For example, changing the crystallisation solvent can result in multiple polymorphs for the same cage molecule, each possessing different physical properties.[9] The inherent solubility of POCs also opens up the possibility of forming cage co-crystals, which can possess tuneable properties[10] and afford access to unique crystal packings.[11]

Typically, organic cages are synthesised from one or two precursors that are able to self-assemble: for example, the imine-based organic cage **CC3**-*R* is synthesised by the reaction of four molecules of 1,3,5-triformylbenzene with six molecules of (*R*,*R*)-1,2-cyclohexanediamine. The precise size and shape of the resulting cage is sensitive to the choice of starting material and the position of the reactive groups with respect to one another,[7,8] and the assembly mode is not always intutive. For this reason, we have developed computational strategies to predict the reaction outcome *in silico*.[12,13] For dynamic systems,[14] reversible bond formation enables error correction during synthesis and can often afford clean formation of the desired cage. To synthesise cage molecules with different shapes or topologies, it is common to use precursors with different geometries.[7,8] It is relatively rare to see changes in cage geometry and/or topology by simply changing the reaction conditions for the same starting materials. However,

rearrangement of imine-based cages in solution to form alternative molecular species is possible because of the dynamic nature of the imine bonds, which can allow equilibration of the reaction mixture in response to external stimuli. Hence, the product distribution may be affected by changes in the reaction conditions, such as temperature, concentration, solvent composition, the presence of a catalyst, or the presence of a templating species.[15] Warmuth demonstrated that solvent can have a strong influence on the outcome of the cage-forming reaction between tetraformylcavitand and ethylenediamine.[16] Simply switching the reaction solvent between chloroform, tetrahydrofuran, or dichloromethane prompted the formation of octahedral [6+12], tetrahedral, [4+8], or square antiprismatic [8+16] nanocages, respectively.[16,17] We also observed that re-crystallizing the tetrahedral [4+6] cage, **CC1**, from DCM with *o*-xylene led to the formation of the thermodynamic triply interlocked [8+12] catenated species.[18] By using TFA as a catalyst, it was possible to form the [8+12] catenane directly in the synthesis.[18] The ability to switch the stoichiometry of the cage products demonstrates that the energetics of host-solvent interactions can be used to fine tune the outcome of a particular synthesis; this is similar to the amplification effect observed in dynamic combinatorial receptor libraries.[19,20] Here we show that two distinct organic cages, **TCC1**$_{[3+6]}$ and **TCC1**$_{[6+12]}$, could be synthesised from the same precursors and that **TCC1**$_{[3+6]}$ is able to undergo re-equilibration to a larger species, **TCC1**$_{[6+12]}$, with only mild experimental stimuli (**Scheme 1**).

RESULTS AND DISCUSSION

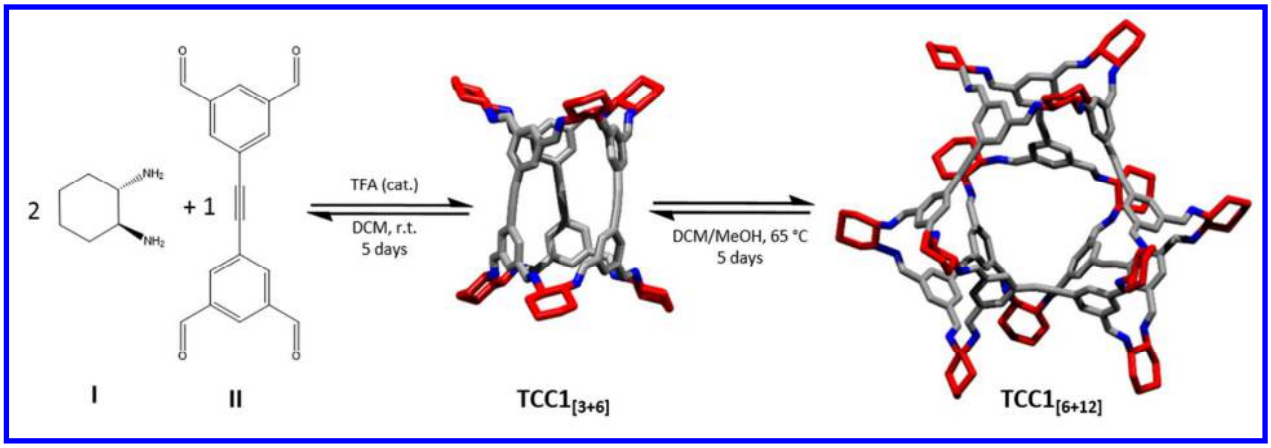

Scheme 1 Reaction scheme for the formation of **TCC1**$_{[3+6]}$, which then re-equilibrates in solution to **TCC1**$_{[6+12]}$, this reaction can be influences by a number of factors detailed in the text. The cyclohexane groups are shown in red; other C, grey; N, blue; H omitted for clarity in the crystal structure representation.

We recently reported a family of chiral cage molecules with a triangular prism shape (the topology can be denoted $\mathbf{Tet_3^3Di^6}$, according to our recently introduced nomenclature)[21], referred to here as **TCC1**$_{[3+6]}$, **TCC2**$_{[3+6]}$, and **TCC3**$_{[3+6]}$ (**Figure S1**)[22]. The smallest cage in this family, **TCC1**$_{[3+6]}$, was shape persistent and found to have an apparent BET surface area (SA_{BET}) of 2037 m^2g^{-1} as a homochiral crystalline material. In a subsequent crystallization screen for **TCC1**$_{[3+6]}$, we observed a new crystal habit for this system. Crystallization of **TCC1**$_{[3+6]}$ from a chloroform solution containing ethanol or methanol as an antisolvent afforded a mixture of acicular or needle-like crystals, along with the previously observed crystals of **TCC1**$_{[3+6]}$, which are cubes. The needles were found to be single, although some non-merohedral twining was observed. Single crystal X-ray diffraction (SCXRD) revealed the presence of a large cage, **TCC1**$_{[6+12]}$ (**Scheme 1**). While **TCC1**$_{[3+6]}$ has a triangular prism geometric shape (**Figure 1a**), **TCC1**$_{[6+12]}$ has a truncated tetrahedron geometric shape ($\mathbf{Tet^6Di^{12}}$ topology) (**Figure 1b**). **TCC1**$_{[3+6]}$ has two triangular shaped windows at either end of the triangular prism-shaped cage,

but **TCC1**$_{[6+12]}$ has four equivalent triangular windows that form the truncated faces of the tetrahedron (**Figure 1c**). In addition, **TCC1**$_{[6+12]}$ has four larger windows that are located between six hexagonally-arranged aromatic rings (**Figure 1d**). Identical crystallisation studies with **TCC2-***R* and **TCC3-***R*, which have longer aldehyde linkers, did not yield any evidence for the formation of an equivalent larger cage (**Figure S1**).

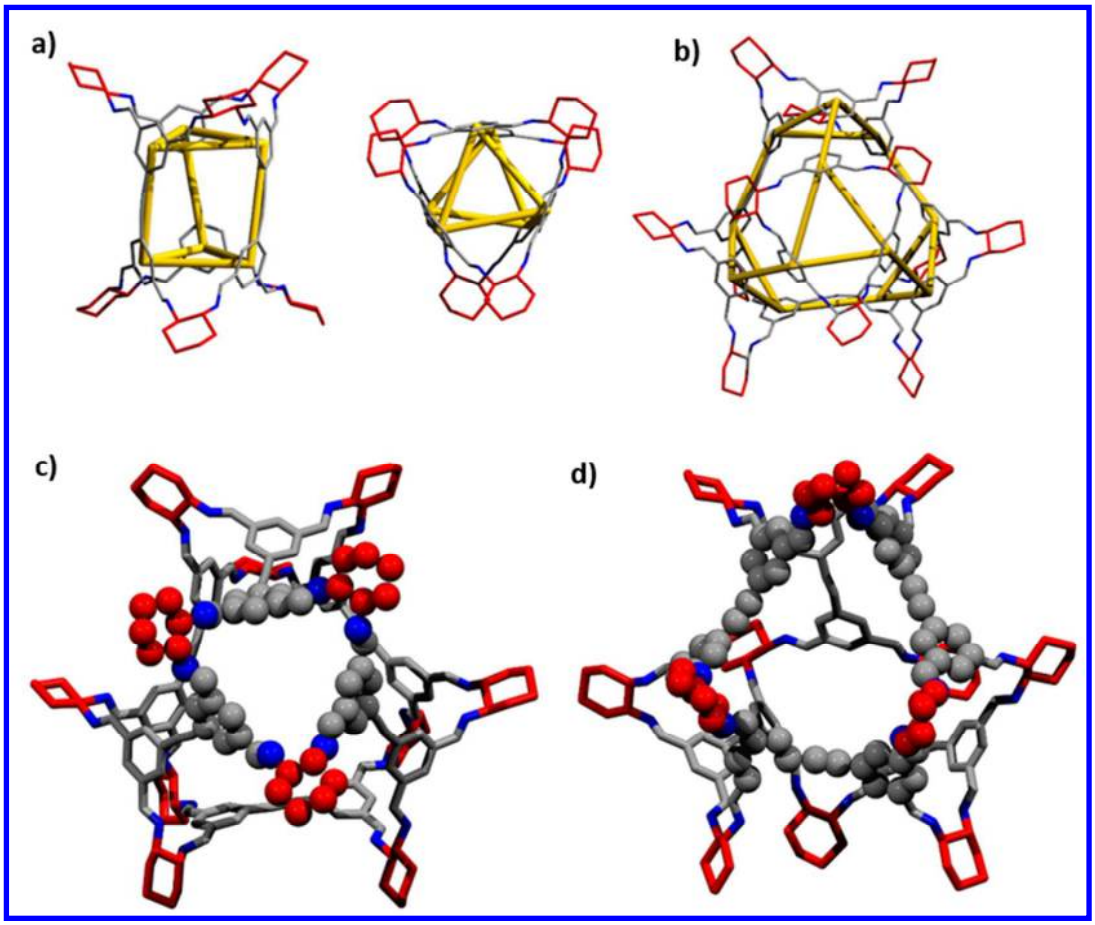

Figure 2 a) Triangular prism geometric shape of **TCC1**$_{[3+6]}$; b) Truncated tetrahedron geometric shape of **TCC1**$_{[6+12]}$; c) Triangular windows of **TCC1**$_{[6+12]}$; d) Hexagonal windows in **TCC1**$_{[6+12]}$. The cyclohexane groups are shown in red; other C, grey; N, blue; H omitted for clarity in the crystal structure representation.

TCC1$_{[6+12]}$ crystallises in the trigonal space group $R3$, a = 38.524(7) Å, c = 18.607(4) Å, V = 23915(10) Å^3 from a $CHCl_3$/EtOH solution as a solvate (**Figure S2–4**, **Table S1**). The smaller cage, **TCC1**$_{[3+6]}$, can also be crystallised from the same solvents but in the cubic space group $I2_13$, a = 29.915(4) Å (**Figure S5**). Calculations in Mercury,[23] using a probe radii of 1.2 Å and grid spacing of 0.15 Å, revealed that the solvated crystal structure of **TCC1**$_{[6+12]}$ has a solvent accessible void volume of 7840 Å^3. Solvent moleclues were extremely disordered in the large void and it was necessary to use the SQUEEZE routine in PLATON during refinment.[24] The structural difference between **TCC1**$_{[3+6]}$ and **TCC1**$_{[6+12]}$ can be understood by examining the orientation of the biphenyl group with respect the triangular shaped window (**Figure 2**, **Table S2**). In **TCC1**$_{[3+6]}$, the biphenyl units are aligned and perpendicular to these windows (**Figure 2a**), whereas in **TCC1**$_{[6+12]}$, they are splayed out in a pyramidal shape to form the larger truncated tetrahedron cage (**Figure 2b**).

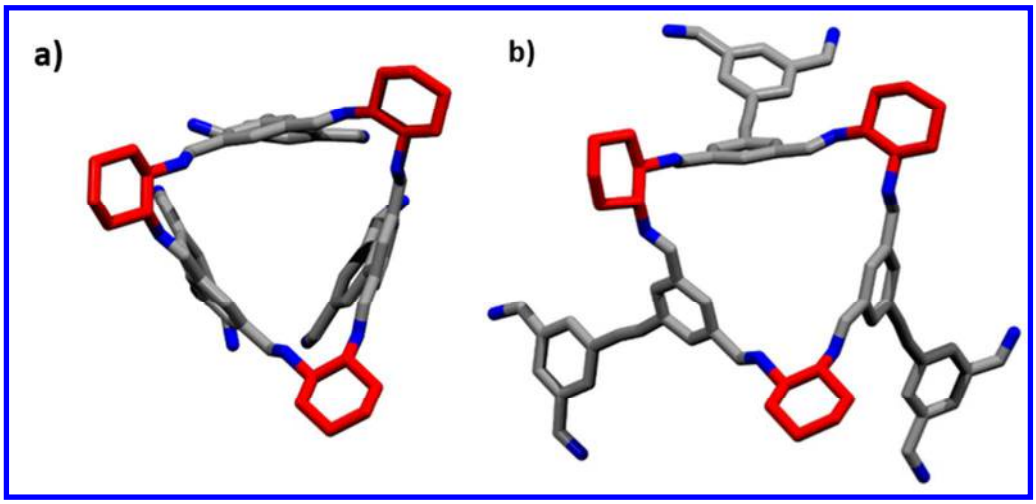

Figure 2 a) View through the triangular window of **TCC1**$_{[3+6]}$; b) View through the isostructural triangular window of **TCC1**$_{[6+12]}$. The cyclohexane groups are shown in red; other C, grey; N, blue; H omitted for clarity.

In the solvated crystal structure of **TCC1**$_{[6+12]}$, the cages pack along the c-axis in a window-to-window configuration, with the smaller, triangular window inserted into the larger, hexagonal windows (**Figure 3a**). These window-to-window interactions form one dimensions chains throughout the crystal structure, although only along one axis (**Figure 3b**).

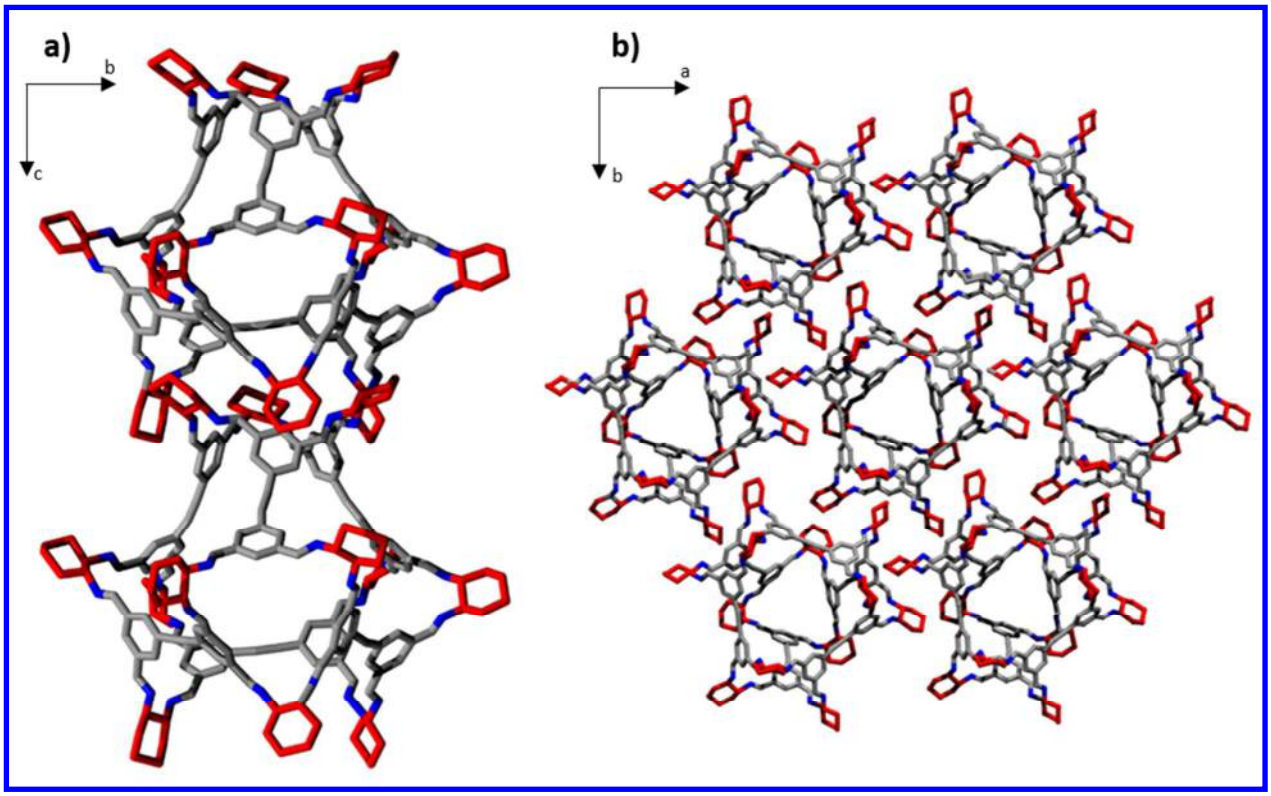

Figure 3 a) Window-to-window interaction between two **TCC1**$_{[6+12]}$ cages, showing the inclusion of the smaller window within the larger window; b) Extended crystal packing of **TCC1**$_{[6+12]}$, illustrating the one dimension chains throughout the structure along the c-axis. The cyclohexane groups are shown in red; other C, grey; N, blue; H omitted for clarity.

HPLC analysis of a **TCC1** crystallisation mixture, which contained both crystal habits, showed the presence of two main peaks, one of which showed the same retention time as the pure **TCC1**$_{[3+6]}$ cage (**Figure S6 & S7**). The new peak, which had a longer retention time, was therefore assigned as **TCC1**$_{[6+12]}$ cage based on Liquid Chromatography Mass Spectrometry

(LCMS) (**Figure S8**). Since crystallisations starting with **TCC1**$_{[3+6]}$ failed to afford a high conversion to **TCC1**$_{[6+12]}$, we attempted to optimise the reaction conditions to favour the formation of the larger cage. The starting point for the synthetic optimisation was the reported procedure for the **TCC1**$_{[3+6]}$ synthesis; characterisation of this material by NMR, MS, HPLC, PXRD, and SEM gave no indication that the original synthesis procedure afforded any **TCC1**$_{[6+12]}$.

Twenty reactions designed to evaluate the effects of temperature, concentration, stoichiometry, and solvent composition were performed in parallel (**Table S3**). Although the original synthetic procedure was performed in dichloromethane,[22] we selected $CHCl_3$ as the primary solvent because the original crystallisation study that afford **TCC1**$_{[6+12]}$ used $CHCl_3$. The reactions were monitored by HPLC, which showed that in addition to the peaks corresponding to **TCC1**$_{[3+6]}$ and **TCC1**$_{[6+12]}$, a third, unidentified peak was also present in most reactions performed in $CHCl_3$ (**Figure S9–13**). We were unable to obtain a definitive mass ion for this peak using LC-MS and, as such, we could not determine whether this third peak represents another cage possessing a different stoichiometry or an intermediate in the cage rearrangement.

There was no substantial increase in the proportion of **TCC1**$_{[6+12]}$ in $CHCl_3$; because of this, and the third unidentified peak in the HPLC, the reactions were repeated in DCM (**Table S4**). HPLC revealed that the use of DCM as the primary solvent afforded better conversion to the large cage while suppressing the formation of the unidentified peak (**Figure S17**). There appears to be a general trend that the more polar the co-solvent, the greater the conversion to the big cage (**Table S5**). The conditions that most favoured formation of the large cage were elevated temperatures with no acid catalyst, a slight excess of the diamine reagent (which often improves reproducibility and overall conversion to the cage product),[25] and low reaction concentrations

around 1 mg ml^{-1}. Our best conditions (1:1 DCM/MeOH, reflux, 5 days, 1 mg/mL, no catalyst) afforded **TCC1**$_{[6+12]}$ with a peak area of 72% by HPLC (**Figures S17**). By comparison, the original published synthesis for **TCC1**$_{[3+6]}$,[22] used an acid catalyst, a more concentrated reaction mixture, and it was performed at room temperature. Isolation of **TCC1**$_{[6+12]}$ was attempted using preparative HPLC and anti-solvent precipitation, but both proved ineffective. This might be due to re-equilibration of the mixture when the solvent composition is changed, or decomposition of **TCC1**$_{[6+12]}$ upon desolvation — we believe that latter is more likely because we were unable to fully dissolve the material after solutions containing **TCC1**$_{[6+12]}$ were evaporated to dryness.

To try to rationalize the formation of **TCC1**$_{[6+12]}$, calculations were performed to compare the relative formation energies of the [6+12] cages with the parent [3+6] cages, **TCC1–3**. To determine the lowest energy conformer for each **TCC1–3** $_{[6+12]}$, structure, the molecules were analyzed in the gas phase using high temperature Molecular Dynamics (MD) combined with the OPLS3 force field.[26] The simulations were run for 100 ns at 1000 K, with a time step of 1 fs, sampling 10000 structures in an NVT ensemble. The simulations were repeated until no new lower energy conformers were generated. The results showed that **TCC1**$_{[6+12]}$ partially collapses (A, teal structure), while **TCC2**$_{[6+12]}$ remains shape persistent with an open internal cavity (B), and **TCC3**$_{[6+12]}$ collapses completely with loss of the internal void (C, teal structure) (**Figure 3**). Nonetheless, it was possible to locate higher energy open conformers for both collapsed structures (A and C, grey structures) and to compare their relative energies with their collapsed equivalents. More thorough energetic and geometric refinements were carried out with Density Functional Theory (DFT) methods on all structures to understand their relative stability. Calculations were performed with CP2K software[27] on both open and collapsed conformers of

all **TCC**$_{[6+12]}$ molecules, using the PBE functional[28] combined with the TZVP MOLOPT basis set,[29] and D3 Grimme dispersion correction. A plane-wave cut-off of 350 Ry was applied.[30]

The open conformer of the large cage, **TCC1**$_{[6+12]}$, was found to be 33 kJ mol^{-1} higher in energy than its partially collapsed equivalent; therefore, it can be expected that this molecule would collapse and lose its internal cavity in the absence of solvent. The molecule is likely to collapse via a vertex-folding mechanism, similar to that postulated for **CC7**;[31] **TCC1**$_{[6+12]}$ contains 12 cyclohexyldiamines, each of which could potentially rotate towards the cavity upon desolvation, thus generating disorder in the crystal structure and a subsequent decrease in porosity. The open conformer of **TCC3**$_{[6+12]}$ was found to be 96 kJ mol^{-1} higher in energy than its completely collapsed conformer. Due to the presence of solvent in the reaction, these cages will most likely assemble as their open conformers; hence, we choose to compare the internal energies of the open **TCC1–3**$_{[6+12]}$ conformers with those of the experimental and simulated **TCC1–3**$_{[3+6]}$ conformers.[32].

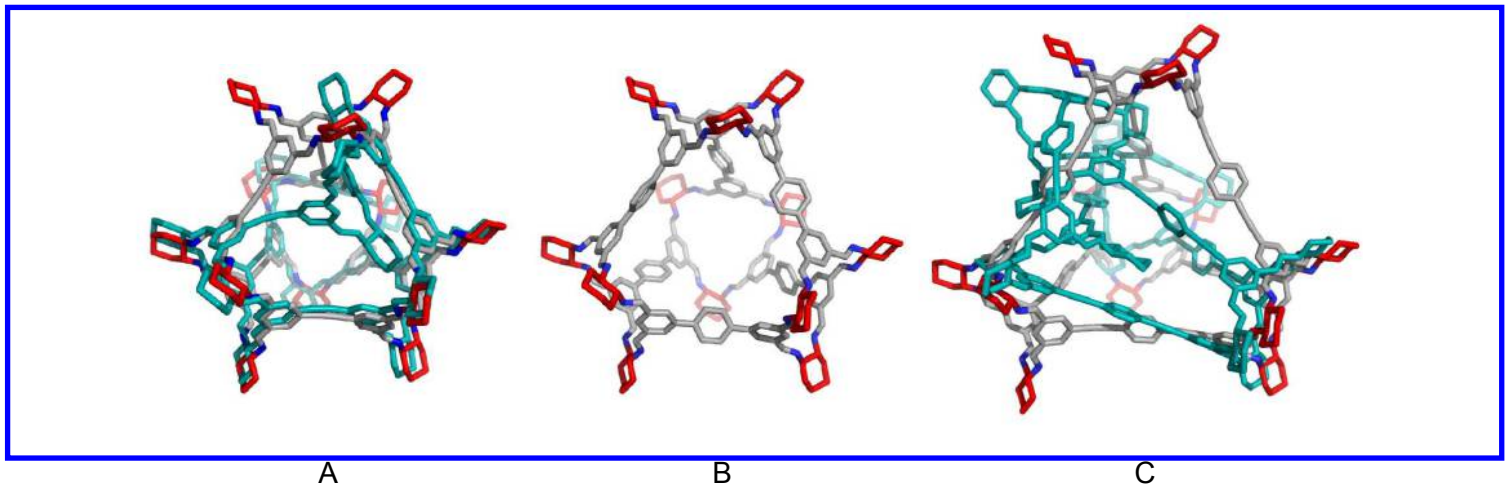

Figure 3 A) **TCC1**$_{[6+12]}$, collapsed (teal) and open structures are overlaid; B) **TCC2**$_{[6+12]}$; C) **TCC3**$_{[6+12]}$, collapsed (teal) and open structures are overlaid

A set of experimental solvated and desolvated crystal structures were available for all three **TCC1–3**$_{[3+6]}$ molecules, as well as a set of manually-constructed molecules for which we carried out a geometry optimisation using DFT. For **TCC1**$_{[3+6]}$, there was little structural difference between these three conformations and, consequentially, their relative energies were similar, but this is not the case for **TCC2** and **TCC3** (**Figure 4**). Our gas phase simulations do not include either solvent or crystal packing effects, hence we do not observe the "swelling" that is seen experimentally in the solvated crystal structures of **TCC2**$_{[3+6]}$ and **TCC3**$_{[3+6]}$. Both the simulated **TCC1**$_{[3+6]}$ and **TCC2**$_{[3+6]}$ structures overlay quite well with the desolvated molecules, with RMSD values of 0.20 and 0.31 Å, respectively. However, the structure of simulated **TCC3**$_{[3+6]}$ twists in a way that is not observed in either the desolvated or solvated crystal structures and it therefore has much poorer RMSDs of 1.98 Å (desolvated) and 3.76 Å (solvated). We attribute this to the absence of crystal packing interactions in our molecular simulations.

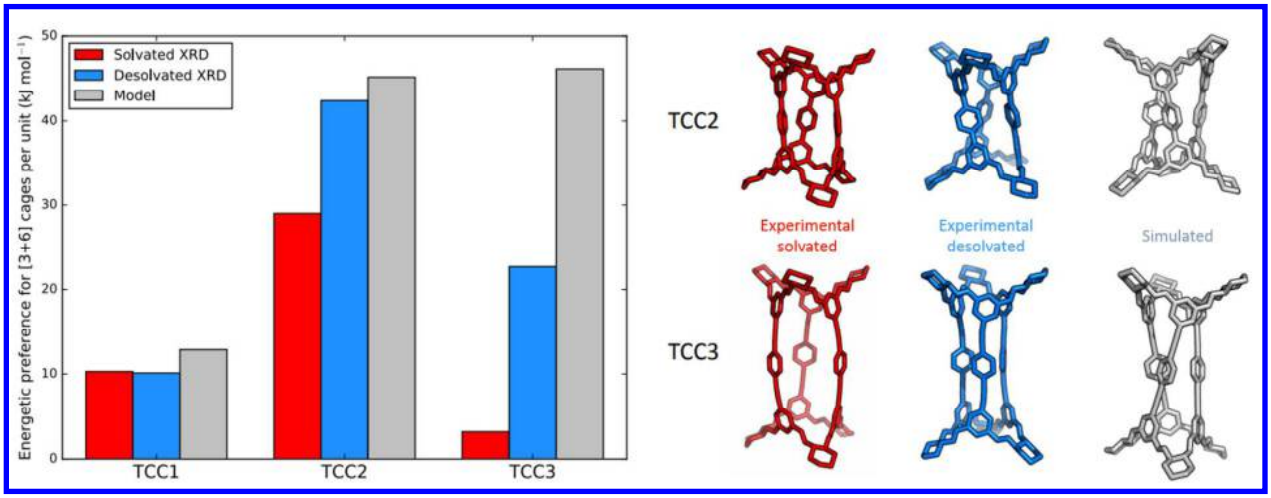

Figure 4 DFT relative stabilities of large **TCC1–3**$_{[6+12]}$ cages with respect to smaller **TCC1–3**$_{[3+6]}$ cages normalized per [3+6] stoichiometric unit; the relative formation energies of open **TCC1–3**$_{[6+12]}$ is 0 in each case (left). The different experimental solvated and desolvated, and simulated crystal structures for **TCC2**$_{[3+6]}$ and **TCC3**$_{[3+6]}$ are shown (right).

We next compared the relative energies of open **TCC1–3**$_{[6+12]}$ and **TCC1–3**$_{[3+6]}$ (simulated, and experimental solvated and desolvated crystal structures) normalized per [3+6] stoichiometric unit (the [6+12] cages being exactly twice the size of the [3+6] molecule). For all three systems, these calculations suggested preferential formation of the smaller [3+6] cages[22] (**Figure 4)**. For **TCC1**, there is only a relatively small energetic difference between the internal relative energy of the [3+6] cages (solvated, desolvated, and simulated) and the open [6+12] cage, of ~10 kJ mol^{-1} per [3+6] stoichiometric unit. The energy difference between the open, solvated [6+12] cage and the [3+6] could potentially be overcome by changes in the reaction conditions, particularly solvent choice.[17] For **TCC2**$_{[6+12]}$, the larger molecule is considerably less energetically favourable than **TCC2**$_{[3+6]}$ by between 29 and 42 kJ mol^{-1}, for the desolvated, solvated, and simulated structures. The situation for the **TCC3** molecule is more complicated because there is a large variation in relative energies between the different conformations. If only the desolvated and simulated conformations are considered, then there is a large preference for **TCC**$_{[3+6]}$ to form by 23 and 45 kJ mol^{-1}, respectively. However, the solvated SCXRD conformation for **TCC3**$_{[3+6]}$ is only 2 kJ mol^{-1} more stable than the open **TCC3**$_{[6+12]}$, which we attribute to the significant strain that is visible in the solvated **TCC3**$_{[3+6]}$ conformation (**Figure 4**). Taken together, these calculated energy differences can rationalize why **TCC1**$_{[6+12]}$ was observed experimentally under certain conditions whereas the equivalent [6+12] analogues of **TCC2**$_{[3+6]}$ and **TCC3**$_{[3+6]}$ were not.

CONCLUSIONS

A new imine cage was isolated by a solvent mediated re-equilibration of a triangular prismatic [3+6] shaped cage to a [6+12] truncated tetrahedron shaped cage. Of the three cages in the **TCC** series, only **TCC1** was found to re-equilibrate in this way. This was rationalised by molecular modelling, which also predicted that the large cage is not shape persistent and would

be expected to partially collapse on desolvation. While the collapsed **TCC1**$_{[6+12]}$ cage was predicted to be lower in energy than **TCC1**$_{[3+6]}$, the open, solvated **TCC1**$_{[6+12]}$ cage was predicted to be higher in energy. Our inability to cleanly isolate **TCC1**$_{[6+12]}$ suggests that the difference in energy between the large and small cages is small. These findings emphasize that subtle changes in crystallization or reaction conditions can have a pronounced effect on the structure of POCs synthesised by reversible bond forming reactions. The results also highlight the importance of characterizing the reaction products by more than SCXRD alone.

ACKNOWLEDGEMENTS

The authors acknowledge the European Research Council under the European Union's Seventh Framework Programme (FP/2007-2013)/ERC through grant agreements n. 321156 (ERC-AG-PE5-ROBOT). KEJ thanks the Royal Society for a University Research Fellowship.

SUPPORTING INFORMATION

Supporting information available for this manuscript contains: Figure S1: Crystal structures of cages **TCC1**–**3** and the structure or their respective aldehyde linkers. Figure S2: Displacement ellipsoid plot for **TCC1**$_{[6+12]}$. Figures S3–5 Crystal packing of **TCC1**$_{[3+6]}$ and **TCC1**$_{[6+12]}$. Table S2: Bond lengths and angles of **TCC1**$_{[3+6]}$ and **TCC1**$_{[6+12]}$ compared to other crystal structures. Figure S6 Microscope image of crystals immersed in oil. Figure S7: Chromatograph of the mother liquor from the crystallisation. Figure S8 LCMS data (a) total ion count (bi & ii) Accurate mass spectra for the small and large cages respectively. Table S3: Synthetic optimization using $CHCl_3$. Figures S9–13: Chromatographs to illustrate the influence of $CHCl_3$ on the reaction. Table S4: Synthetic optimization using DCM. Figures S14–17: Chromatographs to illustrate the influence of DCM on the reaction. Table S5: Influence of polarity on the amount of **TCC1**$_{[6+12]}$. Figure S18: Overlay of the modelled and crystal structure of **TCC1**$_{[6+12]}$.

REFERENCES

(1) Tozawa, T.; Jones, J. T. A.; Swamy, S. I.; Jiang, S.; Adams, D. J.; Shakespeare, S.; Clowes, R.; Bradshaw, D.; Hasell, T.; Chong, S. Y.; Tang, C.; Thompson, S.; Parker, J.; Trewin, A.; Bacsa, J.; Slawin, A. M. Z.; Steiner, A.; Cooper, A. I. Porous organic cages. *Nat Mater* **2009**, *8*, 973.

(2) Li, H.; Eddaoudi, M.; O'Keeffe, M.; Yaghi, O. M. Design and synthesis of an exceptionally stable and highly porous metal-organic framework. *Nature* **1999**, *402,* 276.

(3) El-Kaderi, H. M.; Hunt, J. R.; Mendoza-Cortés, J. L.; Côté, A. P.; Taylor, R. E.; O'Keeffe, M.; Yaghi, O. M. Designed synthesis of 3D covalent organic frameworks. *Science* **2007**, *316*, 268.

(4) Giri, N.; Del Pópolo, M. G.; Melaugh, G.; Greenaway, R. L.; Rätzke, K.; Koschine, T.; Pison, L.; Gomes, M. F. C.; Cooper, A. I.; James, S. L. Liquids with permanenet porosity. *Nature* **2015**, *527*, 216.

(5) McCaffrey, R.; Long, H.; Jin, Y.; Sanders, A.; Park, W.; Zhang, W. Template synthesis of gold nanoparticles with an organic molecular cage. *J. Am. Chem. Soc.* **2014**, *136*, 1782.

(6) Song, Q.; Jiang, S.; Hasell, T.; Liu, M.; Sun, S.; Cheetham, A. K.; Sivaniah, E.; Cooper, A. I. Porous organic cage thin films and molecular-sieving membranes. *Adv. Mater.* **2016**, *28*, 2629.

(7) Hasell, T.; Cooper, A. I. Porous organic cages: soluble, modular and molecular pores. *Nat. Rev. Mater.* **2016**, *1*, 16053.

(8) Zhang, G.; Mastalerz, M. Organic cage compounds — from shape-persitency to function. *Chem. Soc. Rev.* **2014**, *43*, 1934.

(9) Little, M. A.; Chong, S. Y.; Schmidtmann, M.; Hasell, T.; Cooper, A. I. Guest control of structure in porous organic cages. *Chem. Comm.* **2014**, *50*, 9465.

(10) Hasell, T.; Chong, S. Y.; Schmidtmann, M.; Adams, D. J.; Cooper, A. I. Porous organic alloys. *Angew. Chemie Int. Ed.* **2012**, *51*, 7154.

(11) Little, M. A.; Briggs, M. E.; Jones, J. T. A.; Schmidtmann, M.; Hasell, T.; Chong, S. Y.; Jelfs, K. E.; Chen, L.; Cooper, A. I. Trapping virtual porosity by crystal retro-enginerring. *Nat. Chem.* **2015**, *7*, 153.

(12) Jelfs, K. E.; Eden, E. G. B.; Culshaw, J. L.; Shakespeare, S.; Pyzer-Knapp, E. O.; Thompson, H. P. G.; Bacsa, J.; Day, G. M.; Adams, D. J.; Cooper, A. I. In silico design of supramolecules from their precursors: odd-even effects in cage-formaing reactions. *J. Am. Chem. Soc.* **2013**, *135*, 9307.

(13) Briggs, M. E.; Jelfs, K. E.; Chong, S. Y.; Lester, C.; Schmidtmann, M.; Adams, D. J.; Cooper, A. I. Shape prediction for supramolecular organic nanostructures: [4+4] macrocyclic tetrapods. *Cryst. Growth Des.* **2013**, *13*, 4993.

(14) Jin, Y.; Wang, Q.; Taynton, P.; Zhang, W. Dynamic covalent chemistry approaches towards macrocycles, molecular cages, and polymers. *Acc. Chem. Res.* **2014**, *47*, 1575.

(15) Belowich, M. E.; Stoddart, J. F. Dynamic imine chemistry. *Chem. Soc. Rev.* **2012**, *41*, 2003.

(16) Givelet, C.; Sun, J.; Xu, D.; Emge, T. J.; Dhokte, A.; Warmuth, R. Templated dynamic cryptophane formation in water. *Chem. Comm.* **2011**, *47*, 4511.

(17) Liu, X.; Warmuth, R. Solvent effects in thermodynamically controlled multicomponent nanocage syntheses. *J. Am. Chem. Soc.* **2006**, *43*, 14120.

(18) Hasell, T.; Wu, X.; Jones, J. T. A.; Bacsa, J.; Steiner, A.; Mitra, T.; Trewin, A.; Adams, D. J.; Cooper, A. I. Triply interlocked covalent organic cages. *Nat. Chem.* **2010**, *2*, 750.

(19) Mondal, M.; Radeva, N.; Fanlo-Virgós, H.; Otto, S.; Klebe, G.; Hirsch, A. K. H. Fragment linking and optimization of inhibitors of the aspartic protease endothiapepsin: fragment-based drug design facilitated by dynamic combinatorial chemistry. *Angew. Chemie* **2016**, *128*, 9569.

(20) Hamieh, S.; Saggiomo, V.; Nowak, P.; Mattia, E.; Ludlow, R. F.; Otto, S. A "dial-a-receptor" dynamic combinatorial library. *Angew. Chemie Int. Ed.* **2013**, *52*, 12368.

(21) Santolini, V.; Miklitz, M.; Berardo, E.; Jelfs, K. E. Topological landscapes of porous organic cages. *Nanoscale* **2017**, *9*, 5280.

(22) Slater, A. G.; Little, M. A.; Pulido, A.; Chong, S. Y.; Holden, D.; Chen, L.; Morgan, C.; Wu, X.; Cheng, G.; Clowes, R.; Briggs, M. E.; Hasell, T.; Jelfs, K. E.; Day, G. M.; Cooper, A. I. Reticluar synthesis of porous molecular 1D nanotubes and 3D networks. *Nat. Chem.* **2016**, *9*, 17.

(23) Macrae, C. F.; Bruno, I. J.; Chisholm, J. A.; Edgington, P. R.; McCabe, P.; Pidcock, E.; Rodriguez-Monge, L.; Taylor, R.; van de Streek, J.; Wood, P. A. New features for the visualization and investigation of crystal structures. *J. Appl. Crystallogr.* **2008**, *41*, 466.

(24) Spek, A. L. Structural validation in chemical crystallography. *Acta Cryst* **2009**, *65*, 148.

(25) Briggs, M. E.; Cooper, A. I. A perspective on the synthesis, purification, and characterisation of porous organic cages *Chem. Mater.* **2017**, *29*, 149.

(26) Harder, E.; Damm, W.; Maple, J.; Wu, C.; Reboul, M.; Xiang, J. Y.; Wang, L.; Lupyan, D.; Dahlgren, M. K.; Knight, J. L.; Kaus, J. W.; Cerutti, D. S.; Krilov, G.; Jorgensen, W. L.; Abel, R.; Friesner, R. A. OPLS3: a forcefiled providing broad coverage of drug-like small molecules and proteins. *J. Chem. Theory Comput.* **2016**, *12*, 281.

(27) VandeVondele, J.; Krack, M.; Mohamed, F.; Parrinello, M.; Chassaing, T.; Hutter, J. QUICKSTEP: fast and accurate density functional calculations using a mixed Gaussian and plane waves approach. *Comput. Phys. Commun.* **2005**, *167*, 103.

(28) Perdew, J. P.; Burke, K.; Ernzerhof, M. Generalized gradient approximation made simple. *Phys. Rev. Lett.* **1996**, *77*, 3865.

(29) VandeVondele, J.; Hutter, J. Gaussian basis sets for accurate calculations on molecular systems in gas and condensed phases. *J. Chem. Phys.* **2007**, *127*, 114105.

(30) Grimme, S.; Antony, J.; Ehrlich, S.; Krieg, H. A consistent and accurate ab initio parametrization of density functional dispersion correction (DFT-D) for the 94 elements H-Pu. *J. Chem. Phys.* **2010**, *132*, 154104.

(31) Jelfs, K. E.; Cooper, A. I. Molecular simulations to understand and to design porous organic molecules. *Curr. Opin. Solid State Mater. Sci.* **2013**, *17*, 19.

(32) Santolini, V.; Tribello, G. A.; Jelfs, K. E. Predicting solvent effects on the structure of porous organic molecules. *Chem. Comm.* **2015**, *51*, 15542.

For Table of Contents Use Only

Cage Doubling: Solvent-Mediated Re-equilibration of a [3+6] Prismatic Organic Cage to a Large [6+12] Truncated Tetrahedron

Chloe J. Stackhouse, Valentina Santolini, Rebecca L. Greenaway, Marc A. Little, Michael E. Briggs, Kim E. Jelfs and Andrew I. Cooper**

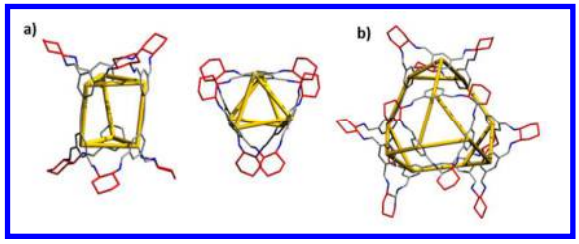

We show that a [3+6] trigonal prismatic imine cage (a) can re-arrange stoichiometrically and structurally to form a [6+12] cage with a truncated tetrahedral shape (b) with double the mass of the smaller cage. Molecular simulations rationalize why this rearrangement was only observed for the prismatic [3+6] cage **TCC1** but not for the analogous [3+6] cages, **TCC2** and **TCC3.**